Eur. Phys. J. A **31**, 233–243 (2007)
DOI 10.1140/epja/i2006-10181-x

THE EUROPEAN PHYSICAL JOURNAL A

Regular Article – Hadron Physics

ω-$\pi\gamma^*$ transition form factor in proton-proton collisions

L.P. Kaptari[a] and B. Kämpfer[b]

Forschungszentrum Rossendorf, PF 510119, 01314 Dresden, Germany

Received: 18 October 2006 / Revised: 22 December 2006
Published online: 5 February 2007 –
Communicated by U.-G. Meißner

Abstract. Dalitz decays of ω and ρ mesons, $\omega \to \pi^0\gamma^* \to \pi^0 e^+e^-$ and $\rho^0 \to \pi^0\gamma^* \to \pi^0 e^+e^-$, produced in pp collisions are calculated within a covariant effective meson-nucleon theory. We argue that the ω transition form factor $F_{\omega\to\pi^0\gamma^*}$ is experimentally accessible in a fairly model-independent way in the reaction $pp \to pp\pi^0 e^+e^-$ for invariant masses of the $\pi^0 e^+e^-$ subsystem near the ω pole. Numerical results are presented for the intermediate-energy kinematics of envisaged HADES experiments.

PACS. 13.60.Le Meson production – 13.75.-n Hadron-induced low- and intermediate-energy reactions and scattering (energy $\leq$ 10 GeV) – 13.85.Lg Total cross-sections – 25.40.-h Nucleon-induced reactions

1 Introduction

The investigation of vector meson production in nucleon-nucleon (NN) reactions represents an interesting topic with various implications. For instance, it is known that the effective repulsive NN forces at short distances can be described, within a boson exchange model, by the exchange of ρ and ω mesons so that a study of their contribution to the NN elastic amplitude and to the meson exchange currents in elastic scattering processes off light nuclei can substantially augment the knowledge of the short-range part of the NN potential. Another important issue of vector meson production in NN collisions is related to electromagnetic probes of strongly interacting systems. As vector mesons carry the $J^P = 1^-$ quantum numbers as the photon, they couple directly to real and virtual photons. The latter ones can be converted into di-electrons in an s-channel process, such allowing a direct access to the spectral distribution of the parent vector meson, even when embedded in strongly interacting matter. (The strong decay channel products would suffer from final-state interaction with the ambient medium. Thus, the di-electron channel serves as direct or penetrating probe [1].)

Furthermore, the decay $\omega \to \pi^0\gamma$ was recently experimentally studied in photo-excitation of nuclei [2]. The difference of the strength distribution of the parent ω for different target nuclei has been ascribed to a medium modification [3]. Such medium modifications are of particular importance for understanding the electromagnetic emissivities of highly excited, strongly interacting systems, *e.g.*, created in the course of relativistic heavy-ion collisions. An extreme option is that the resonances, including the ρ and ω mesons, are molten once the deconfinement and chirally restored phase is entered [4].

Another aspect is to supply information on production of vector mesons in nucleon-nucleon reactions with similar quantum numbers but rather different quark content, such as ω and ϕ mesons [5–8], which is interesting with respect to the Okubo-Zweig-Iizuka rule [9] and hidden strangeness in the nucleon.

A particularly interesting subject is the decay of a vector meson. Besides the above-mentioned direct di-electron decay, $V \to e^+e^-$, where V stands generically for a vector meson, valuable information on the half-off-mass shell decay vertex $V \to \pi\gamma^* \to \pi e^+e^-$ and related transition form factors (FFs) can be obtained. The functional dependence of FFs upon the momentum transfer encodes general characteristics of hadrons, such as charge and magnetic distributions, size etc. The mentioned ω transition FF is related to the ratio of matrix elements $\langle\omega|\pi^0\gamma^*\rangle/\langle\omega|\pi^0\gamma\rangle$.

FFs are also known as important objects for studying bound states within non-perturbative QCD. Theoretical tools for exclusive processes within non-perturbative QCD are approaches based on light cone sum rules and on the factorization theorem (see [10–14] and references therein).

In deep-inelastic scattering processes, an investigation of FFs in a large interval of momentum transfer, including the time-like region, serves as an important tool to provide additional information about the various QCD regimes and on the interplay between soft and hard contributions. For instance, it has been found that the soft part

[a] On leave of absence from Bogoliubov Laboratory of Theoretical Physics 141980, JINR, Dubna, Russia.
[b] e-mail: b.kaempfer@fz-rossendorf.de

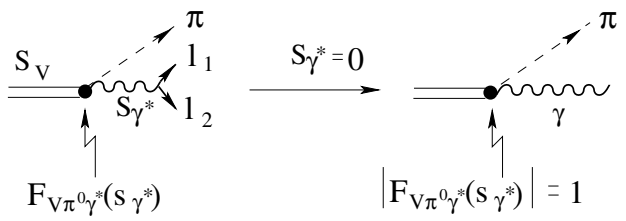

Fig. 1. Left part: Dalitz decay of a vector meson with energy squared s_V into a pion (π) and a di-electron (l_1, l_2). Right part: the transition form factor is normalized at the photon point, *i.e.*, $|F_{V\pi^0\gamma^*}(s_{\gamma^*} = 0)| = 1$.

can be treated as a contribution of configurations in the Fock space with a minimal number of quark constituents. This can be considered as a justification for approaches based on the relativistic quark constituent model for a covariant treatment of mesons as two-particle bound states (see refs. [15,16] for the details of the covariant description of mesons within Bethe-Salpeter–like approaches); correspondingly computed FFs serve as tests of models [15–20].

Besides the mentioned QCD-motivated approaches there is a number of more phenomenological models, *e.g.*, based on the dispersion relation technique [19,21], or on the use of vector meson dominance (VMD) models [22–24] or with effective $SU(3)$ chiral Lagrangians with the inclusion of the non-Abelian anomaly [24–26].

Traditionally, the electromagnetic FFs are studied by electron scattering off stable particles which provides information in the space-like region of momenta where, as well known, the experimental data can be peerless parameterized by dipole formulae. This in turn means that in the unphysical region, *i.e.*, for kinematics unreachable by experiments with on-mass shell particles, the analytically continued FFs exhibit a pole structure. Intensively studied FFs are the ones of the pseudoscalar mesons, chiefly the pion. Light vector meson FFs have received less attention since their experimental determination is more difficult. However, new detector installations, like the spectrometer HADES [27], can detect di-electrons production in proton-proton (pp) collisions in a wide kinematical range of invariant masses with a high efficiency. Thus, a precision study of the transition FF for the $\omega \to \pi^0 e^+ e^-$ process becomes feasible.

The process of vector meson Dalitz decay can be presented as (see fig. 1)

$$V \to P + \gamma^* \to P + e^- + e^+ , \qquad (1.1)$$

where P denotes a pseudoscalar meson. Obviously, the probability of emitting a virtual photon is governed by the dynamical electromagnetic structure of the "dressed" transition vertex $V \to P$ which is encoded in the transition FFs. If the particles V and P were point like, then calculations of mass distributions and decay widths would be straightforward along the standard quantum electrodynamics (QED) technique. Deviations of the measured quantities from the QED predictions directly reflect the effects of the FFs and thus the internal hadron structure, and, consequently, can serve as experimental tests to discriminate the different theoretical approaches.

First experimental measurements of the ω transition FF [28–31] have pointed to a discrepancy with theoretical pre(post)dictions [15,21,25] in the time-like region. Calculations based on VMD do not satisfactorily describe the data. A better description can be achieved with dispersion relation calculations [21] or within models based on the Dyson-Schwinger equation [15]. All these approaches provide rather different transition FFs, with the difference increasing with the momentum transfer. However, the available experimental data is still too scarce for a preferable choice of the approach, and additional data is needed. In this context, forthcoming data from the HADES Collaboration at the heavy-ion synchrotron SIS18/GSI Darmstadt [27] will substantially contribute to our understanding of the problem.

HADES is a detector installation optimized for studies of processes with a e^+e^- pair in one of the final states in reactions of hadrons (p, π) and various nuclei, *i.e.*, pp, πp, Dp, pA, πA, AA etc. near the ρ, ω and ϕ thresholds. In the present paper we study the di-electron production from Dalitz decay of the lightest vector mesons in pp reactions at beam energies of a few GeV for kinematical conditions corresponding to the HADES setup. Our focus is to investigate the transition FF $\omega \to \pi^0 e^+ e^-$. To this end, we calculate the dependence of the differential cross-section for the reaction $pp \to pp\pi^0 e^+ e^-$ upon the invariant mass of the subsystem $\pi^0 e^+ e^-$ around the pole masses of ρ and ω mesons and find a kinematical range where the contribution of ρ is sufficiently small and the cross-section is dominated by Dalitz decays of ω mesons. We calculate the double differential cross-section averaged in a suitable kinematical range as a function of the di-electron invariant mass and argue that such a quantity, normalized to the real photon point and supplemented by some specific kinematical factor, represents the desired transition FF. In such a way a direct experimental investigation of the ω transition FF is feasible.

Our paper is organized as follows. In sect. 2 we introduce the $\omega \to \pi^0 \gamma^*$ transition form factor. Section 3 is devoted to the theoretical background for dealing with the reactions $pp \to pp\omega \to pp\pi^0 e^+ e^-$ and $pp \to pp\rho \to pp\pi^0 e^+ e^-$. Our approach is essentially based on the effective model [5,6] successfully employed in describing the vector (V) meson production in $NN \to NNV$ reactions. The model is based on a phenomenological meson-nucleon theory with parameters adjusted to experiments. Numerical results are presented in sect. 4. The conclusions are summarized in sect. 5, and some formal relations for an integration procedure are relegated to the appendix.

2 The transition form factor

Consider the process of a Dalitz decay of a vector meson into a pion and a virtual photon (di-electron) of the type (1.1). The effective Lagrangian describing the vertex

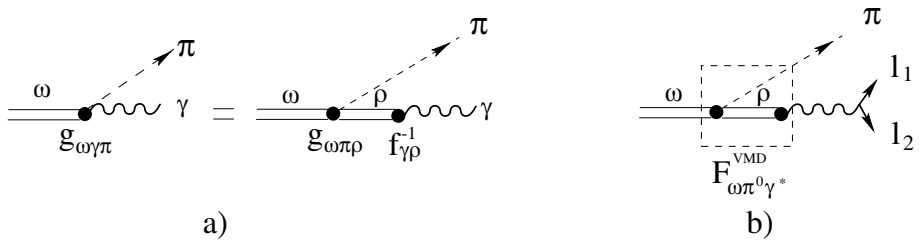

Fig. 2. Diagrams for the calculation of the transition form factor $F_{\omega\pi^0\gamma^*}(s_{\gamma^*})$ within the VMD model. Diagrams in a) correspond to the current-field identity (2.5), while diagram b) is the Dalitz decay within the VMD model.

$V \to \pi^0\gamma$ reads [20,23,24]

$$\mathcal{L}_{V\pi^0\gamma} = f_{V\pi^0\gamma}\left(\epsilon_{\mu\nu\alpha\beta}\partial^\mu A^\nu \partial^\alpha \Phi_V^\beta\right)\boldsymbol{\Phi}_\pi^0\,, \qquad (2.1)$$

where A^ν is the electromagnetic four-potential, Φ_V denotes the neutral vector meson fields ω or ρ, respectively, $\boldsymbol{\Phi}_\pi^0$ stands for the π^0 part of the isovector $\boldsymbol{\Phi}_\pi$ pion field, and $f_{V\pi^0\gamma}$ is the corresponding coupling constant. The fully antisymmetric Levi-Civita symbol $\epsilon_{\mu\nu\alpha\beta}$ is chosen in the standard representation where $\epsilon_{0123} = -1$. The decay width is calculated from (2.1) as

$$\Gamma_{V\to\pi^0\gamma} = \frac{1}{12\pi}\left(\frac{\lambda(s_V,0,\mu_\pi^2)}{4s_V}\right)^{3/2} f^2_{V\pi^0\gamma} \qquad (2.2)$$

and serves for a determination of the coupling constant $f_{V\pi^0\gamma}$ from experimental data. λ is the kinematical triangle function, $\lambda(x,y,z) = (x-(\sqrt{y}-\sqrt{z})^2)(x-(\sqrt{y}+\sqrt{z})^2)$ and the square of the $\pi^0\gamma$ invariant mass is denoted by s_V. Experimentally, the branching ratios Γ_i/Γ_{tot} for $\omega \to \pi^0\gamma$ and $\rho \to \pi^0\gamma$ are known, being $(8.9^{+0.27}_{-0.23})\cdot 10^{-2}$ and $(6.1\pm 0.8)\cdot 10^{-4}$ [32]. Equation (2.2) yields $f_{\omega\pi^0\gamma} \simeq 0.72\,\mathrm{GeV}^{-1}$ and $f_{\rho\pi^0\gamma} \simeq 0.25\,\mathrm{GeV}^{-1}$ for the known total widths $\Gamma_\omega = (8.49\pm 0.08)\,\mathrm{MeV}$ and $\Gamma_\rho = (146.5\pm 1.5)\,\mathrm{MeV}$. The signs of the coupling constants have been chosen positively in agreement with $SU(3)$ symmetry and QCD sum rules (see [22,33]). For the reaction (1.1), however, the emitted photon is virtual and, consequently, the Lagrangian (2.1) must be supplemented by a corresponding transition FF $V \to P$

$$f_{V\pi^0\gamma}(0) \to f_{V\pi^0\gamma}(s_{\gamma^*}) = f_{V\pi^0\gamma}(0)F_{V\pi^0\gamma^*}(s_{\gamma^*}), \qquad (2.3)$$

where s_{γ^*} is the di-electron invariant mass squared. This equation defines the transition FF $F_{V\pi^0\gamma^*}(s_{\gamma^*})$. Direct calculation of the diagram in fig. 1 with the Lagrangian (2.1) results in

$$\frac{\mathrm{d}\Gamma_{\omega\to\pi^0e^+e^-}}{\mathrm{d}s_{\gamma^*}} = \frac{\alpha_{em}}{3\pi s_{\gamma^*}}\frac{\lambda^{3/2}(s_V,s_{\gamma^*},\mu_\pi^2)}{\lambda^{3/2}(s_V,0,\mu_\pi^2)}\Gamma_{\omega\to\pi^0\gamma}\left|F_{\omega\pi^0\gamma^*}(s_{\gamma^*})\right|^2\,, \qquad (2.4)$$

where the part $\frac{\alpha_{em}}{3\pi s_{\gamma^*}}\frac{\lambda^{3/2}(s_V,s_{\gamma^*},\mu_\pi^2)}{\lambda^{3/2}(s_V,0,\mu_\pi^2)}\Gamma_{\omega\to\pi^0\gamma}$ refers to a point-like particle. The mass distribution $\mathrm{d}\Gamma_{\omega\to\pi^0e^+e^-}/\mathrm{d}s_{\gamma^*}$ is determined by i) a purely kinematical (calculable) factor, ii) the decay vertex into a real photon (known from experimental data) and iii) the (yet poorly known) transition FF $F_{\omega\pi^0\gamma^*}(s_{\gamma^*})$. Hence, eq. (2.4) suggests that by measuring the invariant mass distribution one can get direct experimental access to the ω transition FF [28–31].

As mentioned above, the transition FFs are important objects of theoretical calculations for tests and discrimination among the multitude of approaches. The simplest and quite successful theoretical description of FFs can be performed [22,24,25] within the VMD conjecture, and a reasonably good description of elastic FFs in the time-like region has been accomplished. By using the current-field identity [24]

$$J^\mu = -e\frac{M_\rho^2}{f_{\gamma\rho}}\Phi^\mu_{\rho^0} - e\frac{M_\omega^2}{f_{\gamma\omega}}\Phi^\mu_\omega \qquad (2.5)$$

with the coupling constants $f_{\gamma\rho}$ and $f_{\gamma\omega}$ known [34, 35] from experimentally measured electromagnetic decay widths, one can also compute the transition form factor $F^{VMD}_{\omega\pi^0\gamma^*}(s_{\gamma^*})$ by evaluating the corresponding Feynman diagrams (see fig. 2). Contrarily to the elastic case, the FF computed within such an approach exhibits disagreement with data (see below). This immediately implies that with only one (local) FF it is not possible to satisfactorily describe [25,35] the transition vertex, and the simple ρ/ω dominance model must be, at least phenomenologically, supplemented with heavier mesons to modify appropriately the shape of the transition vertex [22].

3 The reaction pp → ppπ^0e$^+$e$^-$

Consider now the di-electron (e^+e^-) production in the exclusive reaction

$$N_1 + N_2 \to N_1' + N_2' + \pi^0 + e^+ + e^- \qquad (3.1)$$

for which the process (1.1) enters as a subreaction. The invariant cross-section is

$$\mathrm{d}^{11}\sigma = \frac{1}{2\sqrt{\lambda(s,m^2,m^2)}}\frac{1}{(2\pi)^{11}}\frac{1}{4} \times\sum_{\text{spins}}|T(P_1',P_2',k_1,k_2,k_\pi,\text{spins})|^2\,\mathrm{d}^{11}\tau_f\frac{1}{n!}, \qquad (3.2)$$

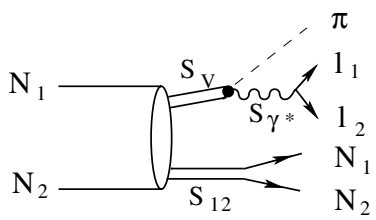

Fig. 3. Illustration of the choice of the independent variables for the process $NN \to NN + \pi + e^+e^-$ within the duplication kinematics [36]. The invariant mass squared of two final nucleons is s_{12}, while the invariant mass of the subsystem πe^+e^- is s_V. The diagram depicted in left part of fig. 1 enters here as a subprocess.

where the factor $1/n!$ accounts for n identical particles in the final state, $|T|^2$ denotes the invariant amplitude squared, and the invariant phase volume $\mathrm{d}\tau_f$ is

$$\begin{aligned}\mathrm{d}^{11}\tau_f = {} & \mathrm{d}s_{12}\mathrm{d}s_V\mathrm{d}s_{\gamma^*}\, R_2(P_1+P_2 \to P_V + P_{12}) \\ & \times R_2(P_{12} \to P_1' + P_2')R_2(P_V \to k_\pi + P_\gamma) \\ & \times R_2(P_\gamma \to k_1 + k_2) \end{aligned} \tag{3.3}$$

with the two-body invariant phase space volume R_2 defined as

$$\begin{aligned}R_2(a+b \to c+d) = {} & \mathrm{d}^4P_c\ \mathrm{d}^4P_d\ \delta^{(4)}\left(P_a + P_b - P_c - P_d\right) \\ & \times\delta\left(P_c^2 - m_c^2\right)\ \delta\left(P_d^2 - m_d^2\right), \end{aligned} \tag{3.4}$$

where P_1, P_2 and P_1', P_2', k_1, k_2, k_π are the four-momenta of the initial and final particles, respectively; m denotes the nucleon mass, while the electron mass can be neglected for the present kinematics. The invariant mass of two particles is hereafter denoted as s. The invariant phase volume $\mathrm{d}\tau_f$ in (3.3) has been chosen within the so-called "duplication" kinematics [36], *i.e.* the one which exploits invariant two-dimensional phase volumes R_2 describing (kinematically) the decay of a real or virtual particle with the invariant mass squared s into two particles, which can also be either real or virtual. This kinematics is schematically depicted in fig. 3.

The invariant amplitude T is evaluated here within a phenomenological meson nucleon theory based on effective interaction Lagrangians which include scalar (σ), pseudoscalar (π), and neutral (ω) and charged/neutral vector (ρ) mesons (see [5–7,37–39])

$$\mathcal{L}_{NN\sigma} = g_\sigma \bar{N} N \Phi_\sigma\,, \tag{3.5}$$

$$\mathcal{L}_{NN\pi} = -\frac{f_{NN\pi}}{m_\pi}\bar{N}\gamma_5\gamma^\mu\partial_\mu(\boldsymbol{\tau}\boldsymbol{\Phi}_\pi)N, \tag{3.6}$$

$$\mathcal{L}_{NN\rho} = -g_{NN\rho}\Big(\bar{N}\gamma_\mu\boldsymbol{\tau}N\boldsymbol{\Phi}_\rho{}^\mu - \frac{\kappa_\rho}{2m}\bar{N}\sigma_{\mu\nu}\boldsymbol{\tau}N\partial^\nu\boldsymbol{\Phi}_\rho{}^\mu\Big), \tag{3.7}$$

$$\mathcal{L}_{NN\omega} = -g_{NN\omega}\left(\bar{N}\gamma_\mu N\Phi_\omega^\mu - \frac{\kappa_\omega}{2m}\bar{N}\sigma_{\mu\nu}N\partial^\nu\Phi_\omega^\mu\right), \tag{3.8}$$

$$\mathcal{L}_{\rho\pi\omega} = g_{\rho\pi\omega}\,\varepsilon_{\mu\nu\alpha\beta}\,\partial^\mu\Phi_\omega^\nu\,\mathrm{Tr}\left(\partial^\alpha\Phi_\rho^\beta\Phi_\pi\right), \tag{3.9}$$

where N and Φ denote the nucleon and meson fields, respectively, and boldface letters stand for isovectors. All couplings with off-mass shell particles are dressed by monopole form factors $F_M = (\Lambda_M^2 - \mu_M^2)/(\Lambda_M^2 - k_M^2)$, where k_M^2 is the four-momentum of a virtual particle with mass μ_M. At kinetic energies near ρ, ω thresholds, contributions from heavier mesons (ϕ, a_1, ...) can be neglected, and we consider first only the Dalitz decays of ρ and ω mesons.

The Lagrangians (3.5)–(3.9) generate two classes of Feynman diagrams: i) the ones which describe the Dalitz decay of a vector meson created from nucleon bremsstrahlung due to NN interaction (via a one-boson exchange potential), see fig. 4a, and ii) Dalitz decay of a vector meson, ω or ρ, from a conversion of virtual π and ρ (or π and ω) exchange bosons into an intermediate vector meson, *i.e.*, from the internal $\rho\pi\omega$ vertex, see fig. 4b. The result of a calculation of these diagrams can be cast in the form of a current-current interaction

$$\begin{aligned}T = {} & J_\alpha(12 \to 1'2'V)\left(\frac{g^{\alpha\beta} - \frac{P_V^\alpha P_V^\beta}{P_V^2}}{P_V^2 - M_V}\,\frac{e\,f_{V\pi^0\gamma}}{P_\gamma^2}\right) \\ & \times\left(\epsilon_{\mu\nu\beta\beta'}P_{\gamma^*}^\mu P_V^{\beta'}\,j_\pm^\nu\right), \end{aligned} \tag{3.10}$$

where $j_\pm^\nu = \bar{u}(k_1)\gamma^\mu v(k_2)$ is the electromagnetic current of the final lepton pair, and $J_\alpha(12 \to 1'2'V)$ stands for the current corresponding to the vector meson production in the NN interaction, *i.e.*, the Feynman diagrams $NN \to NNV$ [5] with the vector meson lines truncated (cf. fig. 4).

The amplitude T consists of two parts: one ($J_\alpha(12 \to 1'2'V)$) describing the production of vector mesons, and the other one ($\epsilon_{\mu\nu\beta\beta'}P_{\gamma^*}^\mu P_V^{\beta'}\,j_\pm^\nu$) being proportional to the amplitude of Dalitz decays of the produced mesons. This prominent feature of the amplitude allows to substantially simplify the expression for the cross-section. In the square of the amplitude one can separate groups of terms which depend only on a part of variables (connected with decay vertices), and correspondingly the multidimensional integral (3.2) can be partially factorized. Note that the decay part ($\epsilon_{\mu\nu\beta\beta'}P_\gamma^\mu P_V^{\beta'}\,j_\pm^\nu$) can also be written in the form of a current-current interaction $\mathcal{J}_{(\beta)\nu}(V \to \gamma\pi)j_\pm^\nu$. Note also that all these currents are conserved, *i.e.* $P_\mu J^\mu = 0$. These circumstances allow one to reduce the dimension of the integral (3.2) by carrying out some of the integrations analytically. For instance, the summation in the square of the amplitude over the di-electron spins results in a quantity (known as the leptonic electromagnetic tensor, see below) which solely contains the whole dependence upon the momenta of the di-electron. This means that the corresponding integral over $R_2(\gamma \to l_1 + l_2)$ can be evaluated independently of other integrations. Moreover, since $P_{\gamma^*}^2 > 0$ is time like, one can perform the integration in the system where the virtual photon is at rest [37] and where the integration is particularly simple: $R_2 = d\Omega_{\mathbf{k}}^*/8$ and the time components of $l_{\mu\nu}$ vanish. For the leptonic tensor

$$l^{\mu\nu} = 4\left[k_1^\mu P_{\gamma^*}^\nu + k_1^\nu P_{\gamma^*}^\mu - 2k_1^\mu k_1^\nu - \frac{s_{\gamma^*}}{2}g^{\mu\nu}\right] \tag{3.11}$$

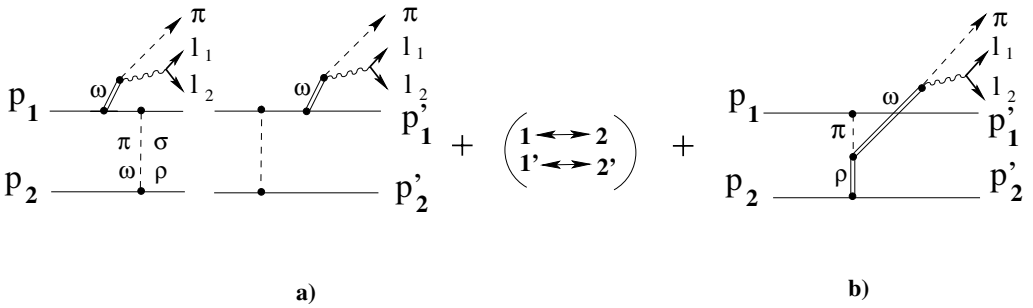

Fig. 4. Diagrams for the resonant part of the process $NN \to NN + \pi + e^+e^-$ within an effective meson nucleon theory with Lagrangians defined by eq. (3.9). a) Dalitz decay of ω mesons from bremsstrahlung diagrams, b) Dalitz decay of ω mesons from internal conversion. Analogous diagrams hold for the ρ meson.

one has

$$\int l^{\mu\nu}(k_1,k_2,P_{\gamma^*})\,\mathrm{d}\Omega^*_{\mathbf{k}} = \frac{16\pi}{3}s_{\gamma^*}\left(-g^{\mu\nu}+\frac{P^\mu_{\gamma^*}P^\nu_{\gamma^*}}{s_{\gamma^*}}\right). \tag{3.12}$$

In a completely analogous way one can integrate over the phase volume $R_2(V \to \pi\gamma)$ (see appendix A). The result is

$$\frac{\mathrm{d}\sigma}{\mathrm{d}s_{\gamma^*}\mathrm{d}s_V} = \frac{1/n!}{2\sqrt{s_0(s_0-4m^2)}}\frac{1}{(2\pi)^{11}}\frac{1}{4} \times \sum_{\substack{\text{nucl.}\\ \text{spins}}}\int |\mathcal{M}|^2 \mathrm{d}^5\tau(s_{12},P_V,P_1',P_2'), \tag{3.13}$$

$$\begin{aligned}|\mathcal{M}|^2 \equiv & \int \sum_{\text{spins}_\pm} |A|^2 R_2(P_V \to P_{\gamma^*}+k_\pi)\; R_2(P_{\gamma^*}\to k_1+k_2)\\ &= \frac{\alpha_{em}}{36}|f_{V\pi\gamma}|^2\frac{(2\pi)^3}{s_V s_{\gamma^*}}\lambda^{\frac{3}{2}}(s_V,s_{\gamma^*},\mu_\pi^2)\\ &\times J_\alpha(NN\to NNV)\left(\frac{-g^{\alpha\beta}+\frac{P_V^\alpha P_V^\beta}{P_V^2}}{P_V^2-M_V^2}\right)\\ &\times J^+_\beta(NN\to NNV),\end{aligned} \tag{3.14}$$

where the phase volume corresponding to the process of pure vector mesons production in the NN interaction, and $\mathrm{d}s_{12}R_2(P_1+P_2\to P_V+P_{12})R_2(P_{12}\to P_1'+P_2')$ is denoted as $\mathrm{d}^5\tau(s_{12},P_V,P_1',P_2')$. In principle, since $P_V^\alpha J_\alpha = 0$, the term proportional to $\frac{P_V^\alpha P_V^\beta}{P_V^2}$ can be omitted. We keep it for further convenience for the interpretation of the results.

4 Results

Expressions (3.14) and (3.13) determine the cross-section for di-electron production within the effective meson nucleon theory. In our calculations of the nucleonic current $J_\alpha(NN\to NNV)$ we use the explicit expressions for the conversion and bremsstrahlung diagrams quoted in ref. [5]. As mentioned above, the Dalitz decay of the ρ meson also contributes as interference effect, so that the current $J_\alpha(NN\to NNV)$ and, consequently, the total amplitude T is a sum of two terms. Since both ρ and ω are not stable the corresponding masses receive imaginary parts, *i.e.*, $M_V \to M_V - iM_V\Gamma_V/2$, where Γ_V is the total decay width of the respective vector meson. The ρ meson decays mainly into two pions. Consequently, its width, as a function of the invariant mass s_V is given by

$$\Gamma_\rho(s_V) = \Gamma_\rho\left(M_\rho^2\right)\frac{M_\rho^2}{s_V}\left(\frac{\sqrt{s_V-4\mu_\pi^2}}{\sqrt{M_\rho^2-4\mu_\pi^2}}\right)^3, \tag{4.1}$$

where $\Gamma_\rho(s_V=M_\rho^2)\approx 0.15\,\mathrm{GeV}$. The width of the ω meson has been kept constant $\Gamma_\omega \approx 0.009\,\mathrm{GeV}$ in the present calculations. Other effective constants entering into the Lagrangians (cut-off form factors, coupling constants, meson masses) have been taken from ref. [5]. The final-state interaction (FSI) among the nucleons has been calculated within the Jost function formalism [40] which reproduces the singlet and triplet phase shifts at low energies. We employ the same formalism as in [38]. In principle, the nearly on-mass shell ω and ρ mesons in the intermediate states can also interact with the nucleons. The magnitude of such corrections has been estimated in ref. [41] by a simulation of rescattering vector mesons off nucleons. The result is that FSI effects from the ω meson rescattering are small. Consequently, due to the finite life time of the ω meson, the reaction product from the Dalitz decay, the pion, is separated in time-space from the nucleons, and effects of πN rescattering in the final state have not been included.

Figure 9 in [42] demonstrates that our model describes fairly precisely the data for the reaction $NN \to NN\omega$ at excess energies 10–300 MeV. The data for the reaction $pp \to pp\rho$ are scarce near threshold, cf. [43]. The application of the present setup (see also [37]) delivers 27.5 (30.8) μb at an excess energy of 300 (330) MeV which compares well with $23.4 \pm 0.8 \pm 8\,\mu$b at an excess energy of 330 MeV [43]. At such excess energy the ρ cross-section is about 2.5 times smaller than the ω cross-section. This can be understood as a result of the interchange of coupling strengths $(g_{NN\rho},\kappa_\rho)$ and $(g_{NN\omega},\kappa_\omega)$ in meson and nucleon currents.

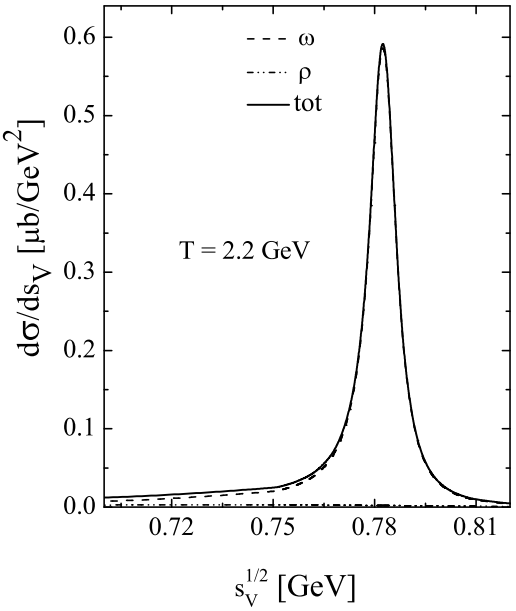

Fig. 5. Differential cross-section $\mathrm{d}\sigma/\mathrm{d}s_V$ for the reaction $pp \to pp + \pi + e^+e^-$ for the kinetic beam energy $T_{beam} = 2.2\,\mathrm{GeV}$. $s_V^{1/2}$ is the invariant mass of the subsystem πe^+e^-. Dashed and double-dot–dashed lines are contributions from decay of ω and ρ mesons, respectively, while the solid line is the total distribution with interference effects. The transition form factors (4.5), entering as input into the calculations, have been computed within the VMD model (see fig. 2).

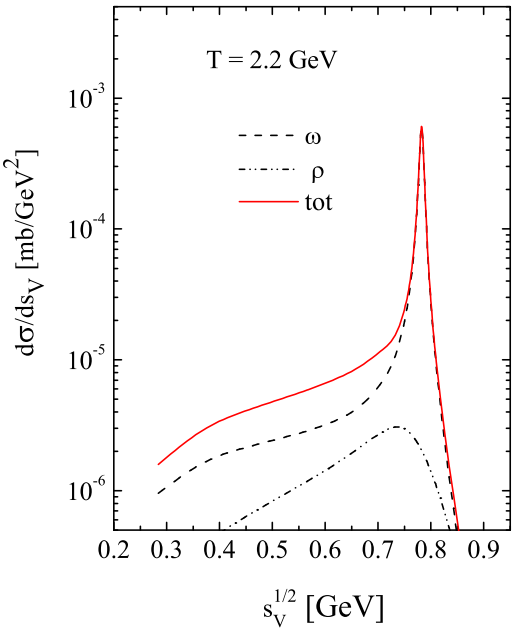

Fig. 6. The same as in fig. 5 but in a log scale. Left to the ω peak the contribution of the ρ meson manifests itself as interference effect.

Results of calculations of the mass distribution $\mathrm{d}\sigma/\mathrm{d}s_V$ are presented in figs. 5 and 6 in linear and log scales, respectively. We have chosen as kinetic beam energy $T_{beam} = 2.2\,\mathrm{GeV}$, similar to the HADES proposal [27]. The dashed line is the contribution from Dalitz decay of ω mesons $\omega \to \pi^0 e^+e^-$, the double-dot–dashed line is the corresponding ρ meson contribution, and the solid curve is the total cross-section, including interference effects as well. It can be seen that in the very vicinity of the ω pole the contribution from ρ mesons is fairly small. This is an understandable result, since the branching ratio for the Dalitz decay of ρ meson is much smaller than that for the ω meson [32]. However, as seen from fig. 6, outside the ω pole mass the interference effects are rather significant. Note that in the direct di-electron bremsstrahlung (two-body channel decay of vector mesons) the contribution of ρ can be competitive with that of ω [37].

The obtained results in figs. 5 and 6 persuade us that for the invariant mass of the πe^+e^- subsystem close to the ω pole mass, the contribution from ρ can be disregarded. This also implies that in the double differential cross-section there is a suitable interval in the vector meson mass s_V in which the contribution from ρ can be neglected.

In fig. 7, results of calculations of the double differential cross-section $\mathrm{d}\sigma/\mathrm{d}s_V\mathrm{d}s_{\gamma^*}$ are presented as a function of the invariant mass squared of the di-electron, s_{γ^*}, in a narrow bin covering the ω meson pole, *i.e.* at mass $s_V \sim M_\omega^2$. It can be seen that in the whole kinematical range of the di-electron invariant mass the double differential cross-section $\mathrm{d}\sigma/\mathrm{d}s_V\mathrm{d}s_{\gamma^*}$ displays a narrow pronounced peak, which is governed by contributions from Dalitz decays of ω mesons. This means that by selecting events with invariant masses s_V of the $e^+e^-\pi$ system in this interval and varying the invariant mass s_{γ^*} of di-electrons, one can experimentally study the process (1.1) in pp collisions. Let us recall in this context the studies [34,

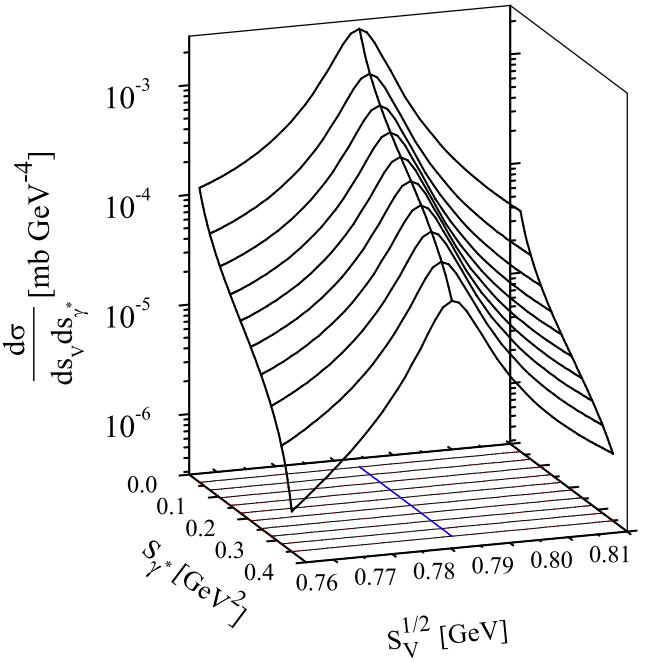

Fig. 7. The double differential cross-section $\mathrm{d}\sigma/\mathrm{d}s_V\mathrm{d}s_{\gamma^*}$ in the vicinity of the ω pole mass $s_\omega^{1/2} = 0.782\,\mathrm{GeV}$ as a function of the di-electron invariant mass squared s_{γ^*}. The interval for the ω mass has been chosen with respect to the envisaged HADES resolution $\sim 3.5\%$ [27].

44], where for the exclusive reaction $\pi N \to N e^+e^-$ the quantum interference of intermediate ρ and ω mesons has been analyzed. In certain kinematical regions this interference is fairly severe and may hamper a clear distinction of $\rho \to e^+e^-$ and $\omega \to e^+e^-$ contributions. In this respect, our calculations support a good prospect to isolate the $\omega \to \pi e^+e^-$ subreaction *vs.* the $\rho \to \pi e^+e^-$ part in the exclusive reaction $pp \to pp\pi^0 e^+e^-$. For a further discussion of interference effects see below.

Let us now focus on the part of the diagrams describing the Dalitz decay of the produced vector mesons in the vicinity of the invariant mass $s_V = s_\omega$. If the contribution from only one vector meson (*e.g.*, the ω meson) is taken into account then, as seen from eqs. (3.14) and (3.13), the cross-section can be presented in the factorized form

$$\frac{\mathrm{d}^2\sigma}{\mathrm{d}s_{\gamma^*}\mathrm{d}s_V} = \frac{\sqrt{s_V}/\pi}{(s_V - M_V^2)^2} \times \int \mathrm{d}^5\sigma^{tot}(NN \to NNV)\,\frac{\mathrm{d}\Gamma(V \to \pi^0 e^+e^-)}{\mathrm{d}s_V}\,, \quad (4.2)$$

where

$$\mathrm{d}^5\sigma^{tot}(NN \to NNV) = \frac{1}{2\sqrt{\lambda(s_0, m^2, m^2)}}\frac{1}{(2\pi)^5}\frac{1}{4} \times \sum_{\substack{\text{nucl.}\\ \text{spins}}}\sum_{\lambda_V} |(J\xi_{\lambda_V})|^2 \mathrm{d}^5\tau(s_{12}, P_V, P_1', P_2') \quad (4.3)$$

is exactly the total cross-section of real vector meson production in NN reactions [5,37]. In eq. (4.3) we formally introduced a polarization vector ξ_{λ_V} which corresponds to a real vector meson V with mass s_V, $\sum_{\lambda_V}\xi^\alpha_{\lambda_V}\xi^{+\beta}_{\lambda_V} = -g^{\alpha\beta} + \frac{P_V^\alpha P_V^\beta}{P_V^2}$. Note that eqs. (4.2) and (4.3) can be easily generalized for contributions from few mesons: in such a case, the cross-section will consist on a sum of two-step–like cross-sections (4.2), corresponding to each meson, and interference terms. In the mentioned kinematical bin our cross-section coincides with the one obtained within a two-step mechanism with one isolated meson. However, outside this kinematical region this is not longer the case, since, apart from interference effects, even the cross-section (4.3) is not anymore an experimentally well-defined quantity, but rather describes the production of a (deeply) virtual vector meson V (see discussion in [37]).

From (2.4), (4.2) and (4.3) it can be seen that the dependence upon the kinematical variables of the subprocesses $NN \to NNV$ and $\omega \to \pi^0 e^+e^-$ can be, in principle, separated in a model-independent way by performing measurements of the double differential cross-section $\mathrm{d}^2\sigma/\mathrm{d}s_{\gamma^*}\mathrm{d}s_V$ keeping the invariant mass s_V constant and varying the di-electron mass s_{γ^*}. In such a way one can extract the transition FF in the same manner as in [28–31]: Define the quantity

$$|F(s_{\gamma^*})|^2 = \frac{s_{\gamma^*}}{s_{min}}\frac{\lambda^{3/2}(s_\omega, s_{min}, \mu_\pi^2)}{\lambda^{3/2}(s_\omega, s_{\gamma^*}, \mu_\pi^2)}\frac{\langle \mathrm{d}^2\sigma/\mathrm{d}s_{\gamma^*}\mathrm{d}s_V\rangle}{\langle \mathrm{d}^2\sigma/\mathrm{d}s_{\gamma^*}\mathrm{d}s_V\rangle|_{s_{\gamma^*}=s_{min}}}\,, \quad (4.4)$$

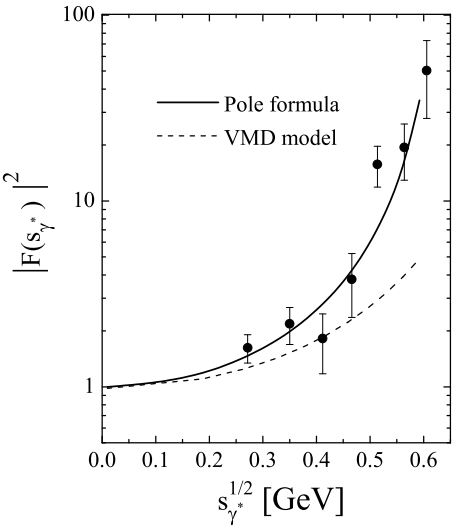

Fig. 8. The ratio (4.4) calculated at $T_{beam} = 2.2\,\mathrm{GeV}$ with two different transition form factors: the dashed line corresponds to the VMD model (4.5), while the solid line is for the dipole formula (4.6). The averaging in (4.4) has been performed in the $\pm 3.5\%$ vicinity of the ω pole mass. Experimental data are from ref. [28].

where $\langle \ldots \rangle$ denotes an average about the ω pole mass corresponding to the experimental mass resolution (say, 3.5% as envisaged for forthcoming measurements at HADES [27]), and $s_{min} = 4m_e^2$ is the minimum value of the di-electron mass which plays a role of a normalization point. Then, as seen from eqs. (2.4) and (4.2), in the kinematical range, where the contribution of Dalitz decays of ρ mesons and interference corrections are negligible, the quantity $F(s_{\gamma^*})$ defined in (4.4) represents indeed the wanted transition FF $F_{\omega\pi^0\gamma^*}$ fairly well.

In fig. 8 the results of calculations of the FF extracted via eq. (4.4) from differential cross-sections are presented for two different choices of parameterizations entering eq. (3.14) with (2.3). The dashed line is the extracted FF with a VMD parametrization for both ρ and ω mesons,

$$F^{VMD}_{\omega\pi^0\gamma^*}(s_{\gamma^*}) = -\frac{M_\rho^2}{s_{\gamma^*} - (M_\rho - \frac{i}{2}\Gamma_\rho)^2}\,,$$
$$F^{VMD}_{\rho\,\pi^0\gamma^*}(s_{\gamma^*}) = -\frac{M_\omega^2}{s_{\gamma^*} - (M_\omega - \frac{i}{2}\Gamma_\omega)^2}\,, \quad (4.5)$$

while the solid line is the result for a pole-like structure of the ω meson FF

$$F^{pole}_{\omega\,\pi^0\gamma^*}(s_{\gamma^*}) = \left(1 - \frac{s_{\gamma^*}}{(0.65\,\mathrm{GeV})^2}\right)^{-1}\,. \quad (4.6)$$

For orientation, the previous experimental data on the ω meson transition FF, extracted from the reaction $\pi^- p \to \omega n \to n\pi^0\mu^+\mu^-$ at pion beam momenta of 25 and $33\,\mathrm{GeV}/c$ [28–31] is also presented in fig. 8. A comparison of the extracted FFs with the corresponding inputs shows that for the considered kinematical conditions they differ by less than 0.5% which demonstrates that, if the

cross-section is really dominated solely by resonant processes with ω and ρ decays alone, the defined ratio (4.4) can indeed serve as a convenient formula to extract the FF from experimental data from pp collisions with high accuracy.

However, actually for the processes of NN scattering with a pion and a di-lepton in the final state, other, non-Dalitz type, diagrams can contribute to the cross-section. In the restricted region $M_{\pi^0 e^+ e^-} \sim M_\omega$ these diagrams play a role of a smooth background and, in principle, can obscure the procedure of extracting FFs by eq. (4.4). To estimate some possible effects of the background one can globally mimic it by one Feynman diagram with production and decay of an effective heavy vector meson into the considered final state with effective (freely adjustable) constants. As seen from eqs. (3.13), (3.14) the structure of the cross-section is

$$\frac{\mathrm{d}\sigma}{\mathrm{d}s_{\gamma^*}\mathrm{d}s_V} \sim -\int \mathrm{d}\Phi(s_{\gamma^*}, s_V, s_{12}, P_i) J_\mu^{(NN\to NNV)} \times \left|\frac{M_V^2}{P_V^2 - (M_V - \frac{i}{2}\Gamma_V)^2}\right|^2 J^{+\mu(NN\to NNV)}, \quad (4.7)$$

where $\mathrm{d}\Phi(s_{\gamma^*}, s_V, s_{12}, P_i)$ is a kinematical function proportional to the phase space volume $\mathrm{d}^5\tau(s_{12}, P_V, P_1', P_2')$, and M_V and Γ_V stand for the mass and width of the effective meson as well. Then it is clear that the resonance structure is governed by the propagator of the ω meson, whereas the sub-diagram $NN \to NNV$ provides a smooth dependence of the cross-section up on s_V. Correspondingly, one can suppose that the background cross-section has the same functional dependence on kinematical variables as the sub-diagram $NN \to NNV$, *i.e.*, it is the same as $J_\mu^{(NN\to NNV)} J^{+\mu(NN\to NNV)}$ with a non-resonant (constant) propagator. As an easily trackable procedure we put the mass of the effective particle $M_V \to M_{bkgr} \gg M_\omega$ and adopt the background cross-section contribution (displayed here without interference terms) in the form

$$\left(\frac{\mathrm{d}\sigma}{\mathrm{d}s_{\gamma^*}\mathrm{d}s_V}\right)^{(bkgr)} \sim -\int \tilde{\Phi}(s_{\gamma^*}, s_V, s_{12}, P_i) \times J_\mu^{(bkgr)} J^{+\mu(bkgr)} \mathrm{d}^5\tau\,, \quad (4.8)$$

where $J_\mu^{(bkgr)} \propto \pm J_\mu^{(NN\to NN\omega)}$, and the function $\tilde{\Phi}(s_{\gamma^*}, s_V, s_{12}, P_i)$ is chosen such that the background at the ω pole is 10%, independent of $s_{\gamma*}$. This order of magnitude can be estimated from available experimental data [28]. Note that the current $J_\mu^{(bkgr)}$, likewise the ω and ρ currents, must be transversal, *i.e.*, $J_\mu^{(bkgr)} P_V^\mu = 0$, which implies that this quantity necessarily depends on kinematical variables, say $J_\mu^{(bkgr)} = J_\mu^{(bkgr)}(s_{\gamma^*}, s_V, s_{12}, P_i)$. This means that this current cannot be parameterized in an arbitrary form; at least the condition $J_\mu^{(bkgr)}(s_{\gamma^*}, s_V, s_{12}, P_i)\ P_V^\mu = 0$ must be fulfilled, as the above choice does. Actually, the amplitude squared entering the cross-section consists of the coherent sum of contributions of ρ and ω and the background

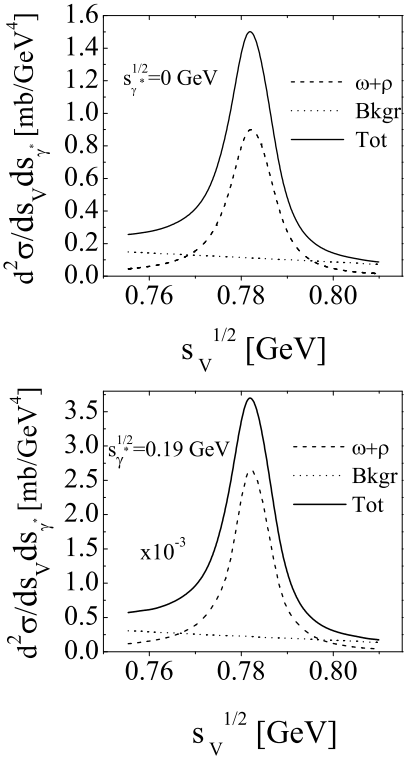

Fig. 9. The double differential cross-section $\mathrm{d}\sigma/\mathrm{d}s_V\mathrm{d}s_{\gamma^*}$ as a function of $s_V^{1/2}$ in the vicinity of the ω pole for $T_{beam} = 2.2$ GeV with background contribution taken into account. The relative sign between the resonant and background amplitudes is chosen positively resulting in a constructive interference. The dashed line corresponds to the resonant contributions of diagrams with ω and ρ Dalitz decays (cf. fig. 7), the dotted line corresponds to the background contribution alone, and the solid line is the resulting total cross-section. The employed transition form factor is for the VMD model eq. (4.5). The top (bottom) panel is for $\sqrt{s_{\gamma*}} = 2m_e \to 0$ (0.19) GeV.

$J_\mu^{(bkgr)} \propto \pm J_\mu^{(NN\to NN\omega)}$ with constant proportionality factor. The phase of the latter one is aimed at bracketing more favorable situations where the background adds up incoherently and may be subtracted in accessing the FF.

In figs. 9 and 10 the results of calculations of the cross-section (3.13) with including the background (4.8) are presented. In fig. 9 the relative sign of the background current is chosen positive (the interference is almost everywhere constructive), whereas in fig. 10 the sign is negative (the interference is mainly destructive). The background (4.8) provides a smooth contribution to the resonant cross-section; at ω peak it is about 10%, as dialed. However, the interference effects are rather important here and can result in corrections up to 55% at large $s_{\gamma*}$. Figures 9 and 10 also demonstrate that in case of a constructive interference the resulting cross-section (solid lines) is always larger than the cross-section without background contributions (dashed lines), whereas in case of a destructive interference the corresponding cross-section is smaller near the peak and larger outside. These circumstances are rather important in the integrated cross-sections since in

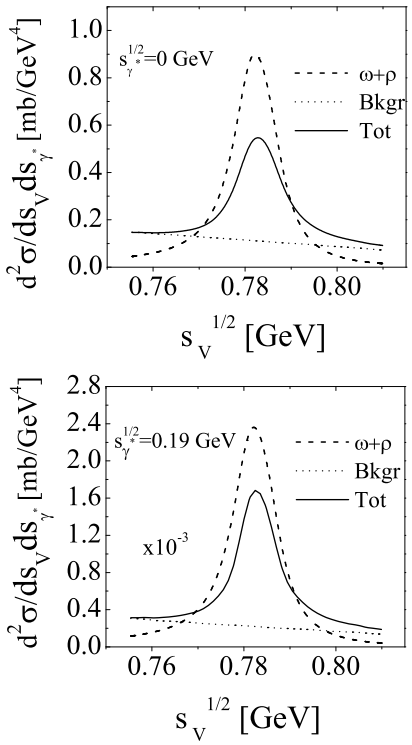

Fig. 10. The same as in fig. 9 but with a destructive interference of resonant and background contributions.

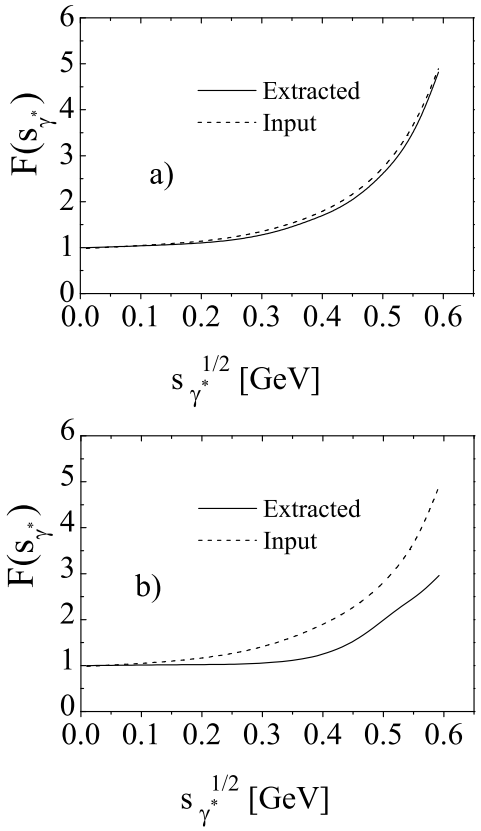

Fig. 11. The extracted FF (solid curves) by using the ratio (4.4) calculated at $T_{beam} = 2.2$ GeV with inclusion of the background contribution. Dashed lines correspond to the input FF taken from the VMD model (4.5). The averaging has been performed in the $\pm 3.5\%$ vicinity of the ω pole mass. Panels a) and b) correspond to destructive and constructive interference effects, respectively.

the latter case the contribution of the background is partially compensated in the integral so that the FF extracted via eq. (4.4) can be quite different in the two cases. This situation is illustrated in fig. 11, where the input FFs and the extracted FFs are compared. One can conclude that a constructive interference of the background may cause some uncertainty in the procedure of the experimental determination of the ω transition FF.

5 Summary

In summary, we have analyzed the di-electron production from Dalitz decays of light vector mesons produced in *pp* collisions at intermediate energies. The corresponding cross-section has been calculated within an effective meson-nucleon approach with parameters adjusted to describe the free vector meson production [5,6] in nucleon-nucleon reactions near the threshold. A possible smooth background contribution to the process has been evaluated as well. Particular attention is paid to the problem of whether it is possible to determine in such reactions the vector meson transition form factors. We argue that by studying the invariant mass distribution of the final πe^+e^- subsystem as a function of the di-electron mass in a narrow kinematical interval near the ω meson mass one can directly measure the ω meson transition form factor $F_{\omega\pi^0\gamma^*}$ in, *e.g.*, *pp* collisions. Such experiments are envisaged at HADES and our results may serve as predictions for these forthcoming experiments. The uncertainties of a procedure to extract $F_{\omega\pi^0\gamma^*}$ depend upon the scale of the background processes and are expected to be small if the interference is destructive. Experimental information on form factors is useful for testing QCD predictions of hadronic quantities in the non-perturbative domain.

We thank H.W. Barz and A.I. Titov for useful discussions. L.P.K. would like to thank for the warm hospitality in the Research Center Rossendorf. This work has been supported by BMBF grants 06DR121, 06DR135 and the Heisenberg-Landau program.

Appendix A. Integration over decay vertices

The decay part $(\epsilon_{\mu\nu\beta\beta'} P^\mu_{\gamma^*} P_V^{\beta'} j^\nu_\pm)$ in eq. (3.10) can be written in the form of a current-current interaction, $\mathcal{J}_{(\beta)\nu}(V \to \pi^0\gamma) j^\nu_\pm$, where $j^\nu_\pm$ is the electromagnetic current of the di-electron, and the decay current is $\mathcal{J}_{(\beta)\nu} \sim \epsilon_{\mu\nu\beta\beta'} P^\mu_{\gamma^*} P_V^{\beta'}$. In the square of the amplitude these currents form the corresponding electromagnetic ($l^{\nu\nu'}$) and decay ($\mathcal{T}_{(\beta\beta')\nu\nu'}$) tensors, respectively. Obviously, both currents, $j^\nu_\pm$ and $\mathcal{J}_{(\beta)\nu}$, and consequently, both tensors

are conserved:

$$P_\gamma^\nu l_{\nu\nu\prime} = P_\gamma^{\nu\prime} l_{\nu\nu\prime} = 0, \qquad P_V^\nu \mathcal{T}_{(\beta\beta\prime)\nu\nu\prime} = P_V^{\nu\prime} \mathcal{T}_{(\beta\beta\prime)\nu\nu\prime} = 0. \tag{A.1}$$

Consider now the integral over the di-electron phase volume. The electromagnetic tensor (3.11) depends only on the momenta of the virtual photon and di electron, so that the Lorentz structure, after integration over $R_2(\gamma \to e^+e^-)$, will be governed by only two terms: one proportional to the metric tensor $g^{\nu\nu\prime}$ and another one proportional to $P_{\gamma^*}^\nu P_{\gamma^*}^{\nu\prime}$:

$$\int l^{\nu\nu\prime}(k_1, k_2, P_{\gamma^*}) R_2(\gamma \to e^+e^-) = a_1 g^{\nu\nu\prime} + a_2 P_{\gamma^*}^\nu P_{\gamma^*}^{\nu\prime}\,. \tag{A.2}$$

Equation (A.1) implies that $a_1 = -a_2 s_{\gamma^*}$. Multiplying (A.2) by $g_{\nu\nu\prime}$, one gets

$$a_2 = -\frac{1}{3}\int [(k_1 P_{\gamma^*}) - s_{\gamma^*}]\,\mathrm{d}\Omega_{\mathbf{k}}^* = \frac{2\pi}{3}\,, \tag{A.3}$$

$$\int l^{\nu\nu\prime}(k_1, k_2, P_{\gamma^*}) R_2(\gamma \to e^+e^-) = \frac{2\pi}{3} s_{\gamma^*}\left(-g^{\nu\nu\prime} + \frac{P_{\gamma^*}^\nu P_{\gamma^*}^{\nu\prime}}{s_{\gamma^*}}\right). \tag{A.4}$$

Analogously, one has for the decay tensor $\mathcal{T}_{(\beta\beta\prime)\nu\nu\prime}$

$$\int \epsilon_{\mu\nu\alpha\beta}\epsilon_{\mu\prime\nu\alpha\prime\beta\prime} P_{\gamma^*}^\mu P_{\gamma^*}^{\mu\prime} P_V^\alpha P_V^{\alpha\prime} R_2(P_V \to k_\pi + P_{\gamma^*}) = a_1 g^{\beta\beta\prime} + a_2 P_V^\beta P_V^{\beta\prime} \tag{A.5}$$

with $a_1 = -a_2 s_V$ and $a_1 = \frac{\pi}{12 s_V}\lambda^{3/2}(s_V, \mu_\pi^2, s_{\gamma^*})$ and

$$\int \epsilon_{\mu\nu\alpha\beta}\epsilon_{\mu\prime\nu\alpha\prime\beta\prime} P_{\gamma^*}^\mu P_{\gamma^*}^{\mu\prime} P_V^\alpha P_V^{\alpha\prime} R_2(P_V \to k_\pi + P_{\gamma^*}) = \frac{\pi}{12 s_V}\lambda^{3/2}(s_V, \mu_\pi^2, s_{\gamma^*})\left(-g^{\beta\beta\prime} + \frac{P_V^\beta P_V^{\beta\prime}}{s_V}\right). \tag{A.6}$$

References

1. R. Rapp, J. Wambach, Adv. Nucl. Phys. **25**, 1 (2000).
2. CB-TAPS Collaboration (D. Trnka *et al.*), Phys. Rev. Lett. **94**, 192302 (2005).
3. R. Thomas, S. Zschocke, B. Kämpfer, Phys. Rev. Lett. **95**, 232301 (2005).
4. K. Gallmeister, B. Kämpfer, O.P. Pavlenko, Phys. Rev. C **62**, 057901 (2000); Phys. Lett. B **473**, 20 (2000).
5. L.P. Kaptari, B. Kämpfer, Eur. Phys. J. A **23**, 291 (2005).
6. L.P. Kaptari, B. Kämpfer, Eur. Phys. J. A **14**, 211 (2002).
7. K. Nakayama, J. Haidenbauer, J. Speth, Phys. Rev. C **63**, 015201 (2000).
8. A. Sibirtsev, J. Haidenbauer, U.-G. Meißner, nucl-th/0512055.
9. S. Okubo, Phys. Lett. **5**, 165 (1963); G. Zweig, CERN Report 8419/TH 412 (1964); I. Iizuka, Prog. Theor. Phys. Suppl. **37/38**, 21 (1966).
10. A.V. Radyushkin, Phys. Rev. D **56**, 5524 (1997); M. Guidal, M.V. Polyakov, A.V. Radyushkin, M. Vanderhaeghen, Phys. Rev. D **72**, 054013 (2005); M. Diehl, Phys. Rep. **388**, 41 (2003).
11. V.M. Braun, A. Lenz, G. Peters, A.V. Radyushkin, hep-ph/0510237; V.M. Braun, A. Lenz, N. Mahne, E. Stein, Phys. Rev. D **65**, 07411 (2002).
12. V.A. Novikov, M.A. Shifman, A.I. Vainshtein, M.B. Voloshin, V.I. Zakharov, Nucl. Phys. B **237**, 525 (1984).
13. N. Isgur, C.H. Llewellyn-Smith, Nucl. Phys. B **317**, 526 (1989).
14. S. Capstick, N. Isgur, Phys. Rev. D **34**, 2809 (1986); S. Godfrey, N. Isgur, Phys. Rev. D **32**, 189 (1985); K.G. Wilson, T.S. Walhout, A. Harindranath, W.-M. Zhang, R.J. Perry, Phys. Rev. D **49**, 6720 (1994).
15. P. Maris, P.C. Tandy, Phys. Rev. C **65**, 045211 (2002); D. Jarecke, P. Maris, P.C. Tandy, Phys. Rev. C **67**, 035202 (2003).
16. A.V. Anisovich, V.V. Anisovich, V.N. Markov, M.A. Matveev, A.V. Sarantsev, Phys. At. Nucl. **67**, 773 (2004).
17. J.P.B.C. de Melo, T. Frederico, Phys. Rev. C **55**, 2043 (1997); B.D. Keister, Phys. Rev. D **49**, 1500 (1994).
18. F. Cardarelli, I. Grach, I. Narodetskii, G. Salme, S. Simula, Phys. Lett. B **359**, 1 (1995).
19. V.V. Anisovich, L.G. Dakhno, M.A. Matveev, V.A. Nikonov, A.V. Sarantsev, hep-ph/0511109; A.V. Anisovich, V.V. Anisovich, V.N. Markov, M.A. Matveev, V.A. Nikonov, A.V. Sarantsev, J. Phys. G **31**, 1537 (2005).
20. A.V. Anisovich, V.V. Anisovich, V.A. Nikonov, Eur. Phys. J. A **12**, 103 (2001) hep-ph/0305216.
21. G. Köpp, Phys. Rev. D **10**, 932 (1974).
22. A. Faessler, C. Fuchs, M. Krivoruchenko, Phys. Rev. C **61**, 035206 (2000); H.C. Dönges, M. Schäfer, U. Mosel, Phys. Rev. C **51**, 950 (1995).
23. H.B. O'Connell, B.C. Pearce, A.W. Thomas, A.G. Williams, Prog. Part. Nucl. Phys. **39**, 201 (1997).
24. U.-G. Meißner, Phys. Rep. **161**, 213 (1988); N.M. Kroll, T.D. Lee, B. Zumino, Phys. Rev. **157**, 1376 (1967).
25. F. Klingl, N. Kaiser, W. Weise, Z. Phys. A **356**, 193 (1996).
26. Ö. Kaymakcalan, S. Rajeev, J. Schechter, Phys. Rev. D **30**, 594 (1984).
27. HADES Collaboration (P. Salabura *et al.*), Acta Phys. Pol. B **35**, 1119 (2004); HADES Collaboration (R. Holzmann *et al.*), Prog. Part. Nucl. Phys. **53**, 49 (2004).
28. L.G. Landsberg, Phys. Rep. **128**, 301 (1985).
29. R.I. Dzhelyadin, S.V. Golovkin, M.V. Gritsuk, D.B. Kakauridze *et al.*, Phys. Lett. B **84**, 143 (1979); **88**, 379 (1979).
30. R.I. Dzhelyadin, S.V. Golovkin, A.S. Konstantinov, V.P. Kubarovski *et al.*, Phys. Lett. B **102**, 296 (1981).
31. V.A. Viktorov, S.V. Golovkin, R.I. Dzhelyadin, V.P. Kubarovski *et al.*, Yad. Fiz. **32**, 998; 1002; 1005 (1980); Phys. Lett. B **94**, 548 (1980).
32. Particle Data Group (S. Eidelman *et al.*), Phys. Lett. B **592**, 1 (2004).
33. Y. Oh, A.I. Titov, T.-S. Harry Lee, nucl-th/0004055; A. Gokalp, O. Yilmaz, Acta Phys. Pol. B **32**, 2021 (2001).
34. M.F.M. Lutz, B. Friman, M. Soyeur, Nucl. Phys. A **713**, 97 (2003).
35. B. Friman, M. Soyeur, Nucl. Phys. A **600**, 477 (1996).
36. E. Byckling, K. Kajantie, *Particle Kinematics* (John Wiley & Sons, 1973).
37. L.P. Kaptari, B. Kämpfer, Nucl. Phys. A **764**, 338 (2006).

38. A.I. Titov, B. Kämpfer, B.L. Reznik, Eur. Phys. J. A **7**, 543 (2000); Phys. Rev. C **65**, 065202 (2002).
39. K. Nakayama, J.W. Durso, J. Haidenbauer, C. Hanhart, J. Speth, Phys. Rev. C **60**, 055209 (1999).
40. J. Gillespie, *Final-State Interactions*, in *Holden-Day Advanced Physics Monographs*, edited by K.M. Watson (Holden-Day, Inc., San Francisco, London, Amsterdam, 1964).
41. M. Büscher *et al.*, *Study of ω and ϕ meson production in the reaction $pd \to dVp_{sp}$ at ANKE*, experiment proposal #75/ANKE, cf. `http://ikpd15.ikp.kfa-juelich.de:8085/doc/Proposals.html`; `www.fz-juelich.de/ikp/anke/doc/Proposals.shtml`.
42. ANKE Collaboration (S. Barso *et al.*), nucl.-ex/0609010.
43. DISTO Collaboration (F. Balestra *et al.*), Phys. Rev. Lett. **89**, 092001 (2002).
44. A.I. Titov, B. Kämpfer, Eur. Phys. J. A **12**, 217 (2001).